Available online at www.sciencedirect.com
ScienceDirect
Polymer 48 (2007) 2098–2108
polymer
www.elsevier.com/locate/polymer

Foaming behaviour and cellular structure of LDPE/hectorite nanocomposites

J.I. Velasco [a,*], M. Antunes [a], O. Ayyad [a], J.M. López-Cuesta [b], P. Gaudon [b], C. Saiz-Arroyo [c], M.A. Rodríguez-Pérez [c], J.A. de Saja [c]

[a] *Centre Català del Plàstic, Departament de Ciència dels Materials i Enginyeria Metal lúrgica, Universitat Politècnica de Catalunya, C/Colom 114, E-08222 Terrassa (Barcelona), Spain*
[b] *Centre de Recherche Matériaux de Grande Diffusion, Ecole des Mines d'Alès 6, Avenue de Clavières, 30319 ALÈS, Cedex, France*
[c] *Departamento de Física de la Materia Condensada, Cristalografía y Mineralogía, Facultad de Ciencias. Universidad de Valladolid. Prado de la Magdalena s/n, E-47011 Valladolid, Spain*

Received 14 July 2006; received in revised form 10 November 2006; accepted 7 February 2007
Available online 9 February 2007

Abstract

This paper presents the compared analysis of the foaming behaviour and cellular structure of LDPE/hectorite nanocomposites and respective neat LDPE foams. To assess the influence of hectorite on the foaming behaviour and final foam morphology, nanocomposites containing 3 and 7 wt.% of a modified hectorite were first melt-compounded in a twin-screw extruder. Variables such as temperature, pressure and time were optimized to prepare foams in a second stage by a two-step compression-molding process. Crystallinity and crystal structure of the polymer matrix were determined using X-ray scattering (WAXS) and differential scanning calorimetry (DSC). Clay intercalation/exfoliation was analyzed by WAXS and transmission electron microscopy (TEM), with the results indicating that partial exfoliation of the particles was only reached with foaming but not during melt mixing. A quantitative characterization of the cellular structure and morphology of the foamed nanocomposites was done using both scanning (SEM) and transmission electron microscopies. The nanocomposite foams exhibited differences in the crosslinking degree, showing lower gel content values (from 35% of the neat LDPE to as low as 28% for the 7 wt.% hectorite foam), expansion behaviour, cell aspect ratio, with the foamed nanocomposites showing more isometric type of cells, and cell wall texture with regard to the neat LDPE foams. All these differences, analyzed and compared for the three composites, directly affect both the thermal and mechanical responses of the foams and due to that fact are of extreme importance.

Keywords: LDPE; Foams; Nanocomposites

1. Introduction

Polymer/layered silicate nanocomposites have recently attracted great interest, often showing remarkable improvements when compared to the respective virgin polymer or micro-composite. Improvements include higher moduli, tensile strength and heat resistance [1–6], decreased gas permeability [7–9] and flammability [10–13]. On the other hand, the preparation and structure of these materials are also considered to be of extreme importance [14–22], mainly the way to produce exfoliated-clay type polymeric nanocomposites and how their structure relate to the mechanical properties, due to the large surface area of the exfoliated particles and their contact with the polymer matrix [23]. This intimate contact also allows the study of the dynamics of polymer molecules in confined environments [24–26].

Several techniques can be applied to produce polymer–clay nanocomposites [23]. Amongst them, the most used ones are the *in situ* polymerization [23], in which a given monomer is mixed with a clay and then polymerized *in*

* Corresponding author. Tel.: +34 937837022; fax: +34 937841827.
E-mail address: jose.ignacio.velasco@upc.edu (J.I. Velasco).

0032-3861/$ - see front matter © 2007 Elsevier Ltd. All rights reserved.
doi:10.1016/j.polymer.2007.02.008

situ, allowing the growth of the polymeric chains between the clay platelets, helping to separate them; and the melt-processing method [23], in which the polymer is directly mixed with a chemically modified clay. The melt-mixing method requires a minimum of shear strength during processing, in order not only to mix both components but also to partially exfoliate the clay platelets. Two idealized nanocomposite structures can be obtained after melt mixing: intercalated and exfoliated. Intercalation is observed when a limited portion of polymer molecules is inserted in the interlayer region of the clay. Extensive polymer insertion greatly expands the interlayer distance between the clay platelets, ultimately producing their delamination or exfoliation. As mentioned previously, clay exfoliation results are crucial in order to produce a nanocomposite, that is, a nanometric-scaled clay within a polymer matrix. To study how these differences in clay delamination alter the morphology of the foams is of extreme importance.

Hectorite, alongside montmorillonite, is one of the most commonly used smectite-type layered silicates for the preparation of polymer nanocomposites, because of its high ion exchange capacity and surface area. The difficulty of dispersing a hydrophilic type of material such as hectorite in a highly viscous and hydrophobic polyolefin matrix such as polyethylene can be overcome by replacing the hectorite interlayer cations with long chained alkyl ammonium or phosphonium cations [27–29].

Limited work has been done regarding the study of the foaming of a polymer/layered silicate nanocomposite, defining polymer foam as a two phase material in which air bubbles are entrapped in a continuous macromolecular phase [30]. Nanocomposite foams may be obtained by several methods [31], mainly depending on the type of polymer matrix and foaming agent used. In particular, polyolefin (PO) foams are commercially produced by three different methods [31], dependent on the production process and final shape of the product: (1) extruded polyolefin foams, where a foam is directly obtained at the exit of an extrusion die; (2) crosslinked polyolefin foams, in which a partially crosslinked PO matrix stretches during foaming, minimizing gas escaping; and (3) molded PO foams, where previously extrusion-compounded PO materials (with all the foaming additives, mainly the crosslinking and foaming agents), are foamed in a machine that allows to carefully regulate temperature and pressure (hot-plate press, modified oven, etc.) in order to gradually crosslink and foam the material. This third type of PO foams is usually obtained using chemical blowing agents that decompose inside the press at a given temperature, and single (to produce foams with densities higher than 100 kg/m^3) and two-step foaming processes ($<$100 kg/m^3) are commonly used [32].

Closed-cell polyolefin foams, in which all cells are closed by thin polymer walls, often require, as stated previously, a certain crosslinking degree to allow stability during cell growth and limit the escaping of gas. Both physical irradiation (electrons or gamma irradiation) and chemical crosslinking, by means of peroxide-type free radical reactions, are used commercially [31]. Final foam properties depend on the crosslinking and blowing agents' concentrations, processing conditions, cellular structure and morphology and properties of the base polymer, among others [31,33–36].

Nanocomposite foams may show improved cell morphology, with smaller and more isotropic cells, resulting in enhanced thermo-mechanical properties with respect to the neat polymer foams. Particularly, clay nanoparticles may act as nucleation agents for bubble generation in foams using CO_2 as a physical foaming agent, via batch process [37–39] or by direct extrusion [40–42]. On both cases it was concluded that small amounts of clay nanoparticles greatly reduced the cell size of the foams and increased the cell density. Microcellular foams (showing pores with less than 10 μm in size) could be produced by adjusting the interaction between the polymers, the clay surface and CO_2, as well as the foaming conditions, leading to cost savings and better processing control. Cell nucleation, in which it is known that the size, shape and distribution of the particles affect the efficiency of the nucleation process [43], could be improved considerably if an exfoliated-type of structure is achieved for the clay particles, with finer particles reducing the nucleation energy for the growth of the gaseous phase. This way, cell growth is affected, resulting in more isometric and globally smaller cell sized foams. Alongside the fact that the particles act as a reinforcing agent, this could expand the range of properties of this type of materials (for instance to structural applications) and create mechanically improved foams.

Previous work about crosslinked polyethylene foamed with azodicarbonamide (ADC) as foaming agent was carried out by varying the crosslinking and blowing agent concentrations [44–47]. The expansion ratio decreased with increasing the crosslinking content [48] and cell size reduction was noticed with increasing both the molecular weight and the blowing agent concentration [49]. The reaction kinetics of foamed LDPE/crosslinking agent/ADC systems has been studied [50] and some theories have been developed to predict the foam density of a given formulation [47]. Regarding the effects of nanoparticles in the foaming behaviour of polyolefin-based foams, work has been done mainly concentrating on the influence of the particles in the foam structure using CO_2 direct foaming extrusion. It was found that small amounts of clay particles suppress the cell coalescence nature of some polymers, like linear polypropylene, related to its low viscosity and weak melt strength [51–53].

In this paper, crosslinked LDPE/hectorite nanocomposite closed-cell foams were prepared by a two-step compression-molding process and studied, focusing on their foaming behaviour, and characterized in terms of final foam densities and expansion behaviour, cell structure and crystalline characteristics. The influence of foaming on the dispersion of the hectorite particles within the LDPE matrix, as well as how this delamination affects the final foam characteristics, ultimately relating to the global behaviour of the produced materials, is presented and compared to the neat LDPE foams.

2. Experimental

2.1. Materials and compounding

First of all, a low density polyethylene (LDPE), Stamylan LD 2404A (100.00 parts per hundred of resin, phr), manufactured by Sabic Europetrochemicals®, was compounded using a two-roll mill at a constant temperature of 120 °C and constant speed of 60 rpm for not more than 5 min with dicumyl peroxide (DCP, 1.70 phr) used as crosslinking agent; stearic acid (0.11 phr) as a lubricant; azodicarbonamide (ADC, 18.50 phr) as chemical blowing agent; and zinc oxide (0.075 phr) as ADC activator. The LDPE used was a low density polyethylene with a density of 0.925 g/cm^3 and melt flow index (MFI) of 4.2 g/10 min at 190 °C and 2.16 kg. An organic derivative of hectorite (Bentone 108, from Elementis Specialties Inc.), chemically modified with dimethyl dehydrogenated tallow ammonium chloride (2M2HT), with a density of 1.7 g/cm^3, basal spacing (d_{001}) of 2.5 nm and an average specific area of 700 m^2/g, was used.

Secondly, a masterbatch was prepared mixing the powdery hectorite and a compatibilizing polymer in a weight proportion of 1:2 at 160 °C and 160 rpm in a twin-screw extruder (Collin Kneter 25X36D). High density polyethylene grafted with maleic anhydride (Fusabond E MB100D, DuPont), with a density of 0.960 g/cm^3 and MFI of 2 g/10 min at 190 °C and 2.16 kg was used as compatibilizer. These kinds of grafted-modified copolymers are normally used to assist in the formation of polyolefin/clay nanocomposites, enhancing the surface interactions between the non-polar polymer matrix and the organically modified clay [54].

Finally, two composites were prepared using the hectorite masterbatch and part of the previously compounded LDPE, so-called for now on PE0: a 3 wt.% (PE3) and a 7 wt.% (PE7) hectorite composite. The extrudates were water-cooled and pelletized.

2.2. Foaming process

Discs with a nominal diameter of 74 mm and thickness of 3.5 mm were compression-molded in a hot-plate press (IQAP-LAP PL-15). The processed composite pellets were initially placed into a steel mold in order to slightly overfill it and subjected to heating at 110–115 °C for 3 min until melting, followed by a final step at the same temperature and applying a constant pressure of 25 bar for 3 min. The resulting discs were cooled under pressure (25 bar) in the cooling station of the press using recirculating water.

A two-step compression-molding foaming process was used. This process consists of a first step where low temperatures and constant pressures are used in order to gradually crosslink and at the same time start the nucleation of the gas bubbles, favoured at lower temperatures, as well as bubble growth. An expansion ratio of 3 is normally set for the foam expansion at the end of this stage, and the final foam is called a pre-foam. In a second step, higher temperatures are used in order to complete the expansion of the already pre-foamed sample [32].

In this study, the previously prepared solid discs were initially placed in the circular mold and heated at temperatures ranging from 123 °C to 140 °C applying a constant pressure of 40 bar for 90 min. At the end the pressure was released, allowing the foam to partially grow. A typical expansion ratio of 3 was set as the pre-foaming goal. The second step (foaming) consisted of the free expansion (without applying pressure) of the pre-foamed samples at a higher temperature, typically between 140 °C and 180 °C, for not more than 30 min. An expansion ratio of 10 regarding the pre-foam was set.

2.3. Testing procedure

Density of the pre-forms, pre-foams (hereafter referred to as PE0-P, PE3-P and PE7-P, respectively, the pre-foamed compounded polyethylene free of hectorite, the pre-foamed 3 wt.% and the pre-foamed 7 wt.% hectorite nanocomposites) and foams (PE0-F, PE3-F and PE7-F) was measured according to standard procedures [55]. Expansion was carried out at 180 °C under inert atmosphere on initially flat surface pre-foamed samples using a Perkin–Elmer plate setup-like DMA7 in TMA (thermal-mechanical analyzer) mode, in order to measure the horizontal (x,y-direction) and vertical (z-direction) expansions. Cylindrical specimens were prepared for each pre-foamed material with a diameter of 8 mm and an average thickness of 6 mm, with the tests being carried out in the thickness direction. The machine recorded the expansion in the three different directions at the same time, with a minimum of three samples being used to characterize the expansion of each pre-foam.

In order to quantify possible differences regarding the crosslinking degree of the polymer matrix due to the presence of the hectorite particles, the gel content was determined in xylene at 140 °C during 24 h for the foamed nanocomposites, according to standard procedures for crosslinked polyethylene [56]. A minimum of three specimens were tested for each material. Hectorite presence was taken into account when measuring the gel fraction for the different foamed nanocomposites, subtracting the hectorite weight fraction to assess the gel content of the polymer matrix by itself.

The cellular structure of the foams was observed using a JEOL JSM-5610 scanning electron microscope (SEM). Samples were fractured at low temperature and made conductive by sputtering deposition of a thin layer of gold. Low-magnification micrographs were analyzed using the intercept counting method [57], measuring the distance between pairs of cell walls along 10 reference lines, in order to obtain the average cell size (R), cell density and cell shape. The average cell size, being the most used cell structure parameter [30,58–60], was determined using Eq. (1) and applying a correctional value of 1.62 [61], due to the fact that cell sizes were determined in bi-dimensional sections.

$$R = \sum_i m_i f_i \tag{1}$$

where n is the number of analyzed cells, n_i is the number of cells with a size between a_i and b_i, m_i is defined as

$$m_i = \frac{a_i + b_i}{2} \tag{2}$$

and f_i as

$$f_i = \frac{n_i}{n} \tag{3}$$

The aspect ratio (AR), defined as the ratio between the highest and the smallest characteristic cell sizes, was assessed for the different foams using a representative cell population. Average cell wall thickness (t) and mass fraction in the struts (f_s) were two of the main parameters determined from high-magnification micrographs of the samples. The average cell wall thickness (t_{exp}) was calculated first of all using empirical values taken from the thickness of 50 randomly selected cell walls and also using two theoretical models, assuming different cell shapes in a closed-cell foam (t_{theo}): a pentagonal dodecahedron shape (Model 1) and a tetrakaidecahedral cell shape (Model 2). The mass fraction in the struts (f_s^{exp}) was determined using the Gibson and Ashby model [62]. A theoretical model based on the method proposed by Kuhn for pentagonal dodecahedron cells [59] was used as comparison. Cell density was determined for each pre-foamed and foamed sample from the different micrographs using the counting method. A schematic of the cell shapes used in the two models including some of the main cell parameters and the cell-shape constant C is presented in Fig. 1.

Differential scanning calorimetry (DSC) was used to study eventual changes in the thermal characteristics of the polyethylene matrix due to the foaming process and the presence of hectorite particles. A Mettler DSC-30 calorimeter was used with samples weighting around 10 mg, initially heated until 190 °C at 20 °C/min under a constant rate of nitrogen and held for 1 min to erase the thermal history before cooling at 20 °C/min from 190 °C to 30 °C. After a second isothermal step (1 min) at 30 °C, the samples were heated a second time at 20 °C/min from 30 °C to 190 °C to analyze the LDPE melting signal. The melting results were obtained using the 2nd heating curve and both crystallization (c) and melting (m) temperatures relate to the maximum of the peak.

The crystallinity percentage (X_c) was determined according to the following equation:

$$X_c^m(\%) = w_p \frac{\Delta H_m}{\Delta H_m^0} 100 \tag{4}$$

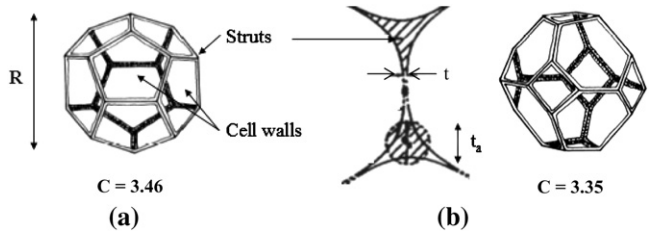

Fig. 1. Schematic of the cell shapes and respective cell-shape constant (C) used to characterize the LDPE foams [59]: (a) pentagonal dodecahedron, (b) tetrakaidecahedron.

where w_p is the weight fraction of LDPE, ΔH_m is the melting enthalpy of the sample and ΔH_m^0 the theoretical, 100% crystalline, polyethylene enthalpy (290 J/g [63]). A minimum of five experiments were done for each material.

Wide-angle X-ray scattering (WAXS) was used to analyze the crystalline characteristics of the pre-formed, pre-foamed and foamed samples. A Bruker D8 diffractometer with Cu Kα radiation, $\lambda = 0.154$ nm, 50 kV and 20 mA was used. Scans were taken from 1° to 30° with a rotation step of 0.05° and a step time of 0.007 s.

Nanocomposite morphology was studied using a HITACHI H-800 transmission electron microscope (TEM) on ultramicrotomed sheets with a typical thickness of 60 nm.

3. Results and discussion

3.1. Foaming behaviour

The expansion behaviour of the three nanocomposite pre-foams and foams is shown as a function of the foaming temperature in Fig. 2 and in Table 1 with the standard deviation values. Globally, the expansion ratio (ER), defined as the ratio between the density of the base polymer (ρ_0) and the density of the foam (ρ_f), increased in both steps for higher foaming temperatures. Hectorite nanocomposites required higher pre-foaming temperatures to reach a similar ER than that of the PE0 foams, due to the fact that the hectorite nanoparticles affected the expansion process by constraining the macromolecules movement as well as decreasing the gas permeation [7–9].

Analyzing the first foaming step, an optimal temperature of 125 °C was established for PE0, which presented both the expansion ratio required (ER ≈ 3), as well as uniform cell structure. For PE3 and PE7 nanocomposites, a value of 140 °C was set as the ideal temperature. The heating of the pre-foams for times higher than 90 min ended in poor cell structure.

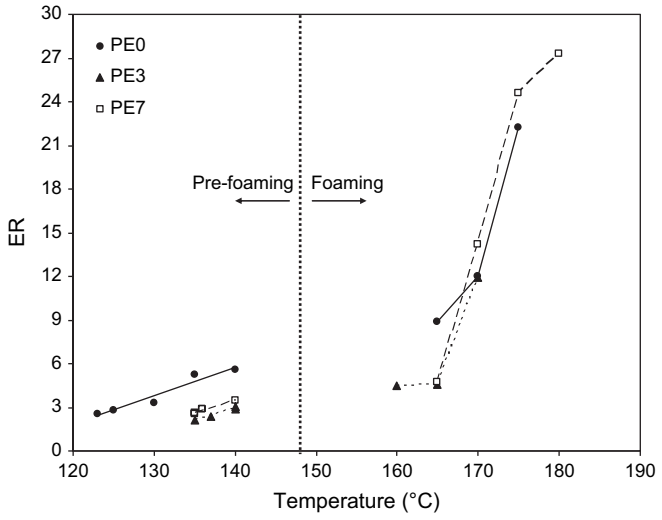

Fig. 2. Expansion ratio versus temperature data obtained from the foaming experiments.

Table 1
Expansion ratio versus temperature data obtained from the foaming experiments (With mean values of density and respective standard deviations)

Material code	Solid disc density (g/cm^3)	Temperature (°C)	Density (g/cm^3)		ER
			Mean value	Standard deviation	
PE0-P	0.925 ± 0.010	123	0.361	0.008	2.6
		125	0.334	0.035	2.8
		130	0.277	0.016	3.3
		135	0.176	0.004	5.3
		140	0.167	0.008	5.5
PE0-F	0.925 ± 0.010	165	0.104	0.009	8.9
		170	0.077	0.008	12.0
		175	0.051	0.015	22.3
PE3-P	0.953 ± 0.012	135	0.444	0.034	2.2
		137	0.401	0.012	2.4
		140	0.330	0.025	2.9
		140	0.309	0.013	3.1
PE3-F	0.953 ± 0.012	160	0.218	0.018	4.5
		165	0.212	0.023	4.6
		170	0.092	0.021	11.9
		175	0.043	0.004	22.2
PE7-P	0.991 ± 0.008	135	0.381	0.021	2.6
		135	0.386	0.012	2.6
		136	0.344	0.014	2.9
		136	0.345	0.010	2.9
		140	0.289	0.008	3.4
PE7-F	0.991 ± 0.008	165	0.209	0.018	4.7
		170	0.070	0.021	14.2
		175	0.042	0.003	24.6
		180	0.036	0.003	27.3

Pre-foaming trials at higher temperatures and lower heating times also resulted in high cell coalescence.

Second step foaming results from the optimized pre-foams are also shown in Fig. 2. The foaming temperature that resulted in the lowest density alongside the best cell structure was found to be around 170 °C for all the composites. The hectorite nanoparticles did not seem to alter the foaming temperature. In conclusion, the hectorite nanoparticles seemed only to affect considerably the early stages of the foaming process (pre-foaming).

Representative curves of the vertical and horizontal expansion with time are shown in Fig. 3. In the *z*-direction (Fig. 3a) an initial shrinkage was observed due to the molecular orientation of the polymer in the pre-foams. This effect was enhanced in PE0 (linear expansion of 33.5%) compared to PE3 (28%) and PE7 (20%), indicating that in the nanocomposites the molecular mobility was restrained due to interactions with the hectorite platelets. In the *x*,*y*-direction (Fig. 3b) this effect was only observed in the PE0 pre-foamed sample (4.7%). After this, PE0 expanded uniformly in both horizontal and vertical directions when compared to the nanocomposites. The ratio between the maximum horizontal expansion and the vertical one, defined here as the expansion uniformity parameter (EUP) was 0.8 for PE0. For perfect uniform expansion EUP would take the value of 1. However, PE3 and PE7 showed EUP values of 2.2 and 2.3, respectively. Thus, the expansion of the nanocomposite pre-foams showed a marked horizontal growth, the cause of which might be related to the pre-foaming process, where the expansion of the solid disc was restrained in the horizontal direction. In addition, these samples reached the maximum expansion at lower times than PE0, and just after this point they started a more abrupt collapsing process. This result was accounted to a lower cross-linking degree of the nanocomposite samples, induced by the hectorite particles, as derived from the values of the gel content presented in Fig. 4.

3.2. Cellular structure

The analysis of the cellular structure for the different pre-foamed and foamed samples was done using the SEM pictures shown in Fig. 5. The characteristic cell parameters are compiled in Table 2. As expected, the average cell size (R) increased with the expansion ratio (ER) and the cell density decreased, as presented in Fig. 6. Both behaviours were found to be independent of the presence of the hectorite particles. So, no evidence of nucleation effect due to the hectorite particles was noticed.

The average cell wall thickness decreased for higher expansion ratios. The two used theoretical models showed lower values of the average cell wall thickness (t_{theo}) compared to the one obtained experimentally (t_{exp}) and also seemed to be independent of the presence of the hectorite particles. Although lower the estimated values, these models can be used

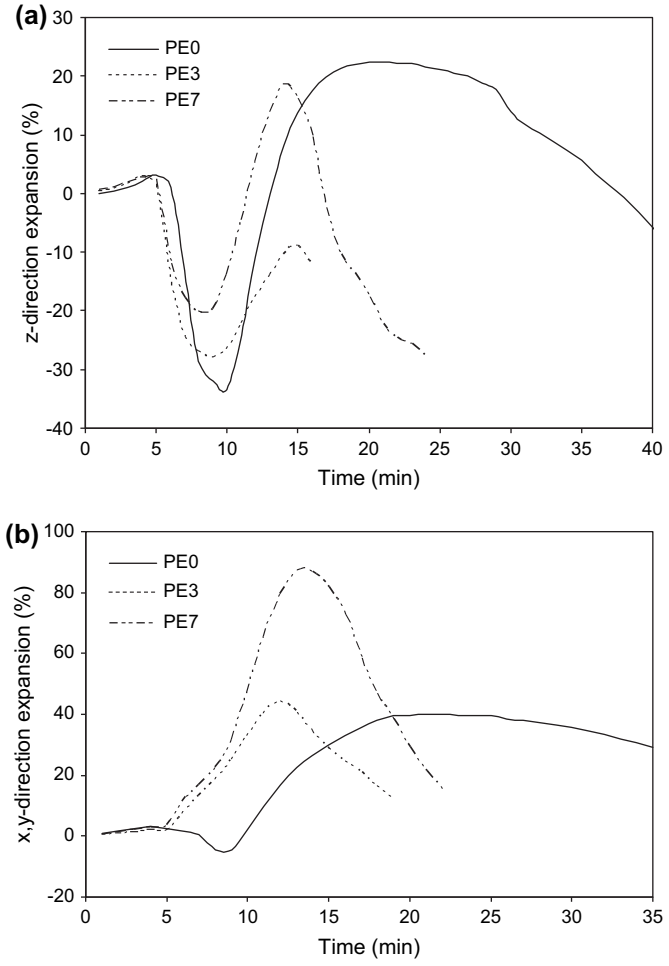

Fig. 3. Expansion behaviour curves at 180 °C for the pre-foams in (a) vertical direction and (b) horizontal direction.

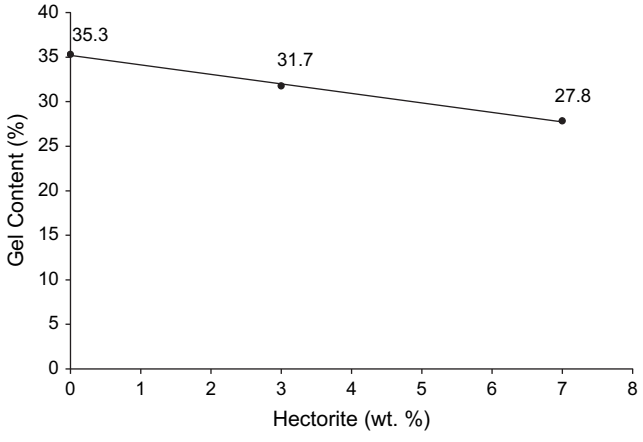

Fig. 4. Gel content of the foamed nanocomposite samples.

to predict cell wall thicknesses in these closed-cell foamed nanocomposites. The foams presented values of mass fraction in the struts (f_s^{exp}) considered typical for closed-cell polymeric foams [62]. Almost no differences were found neither regarding the hectorite nanoparticles nor the ER, as it is shown from the theoretical values obtained assuming pentagonal dodecahedron cells (f_s^{theo}) [59]:

$$f_s^{exp} = \frac{t_a^2}{\left(t_a^2 + \frac{Z_f}{n} t_{exp} l\right)} \tag{5}$$

$$f_s^{theo} = \frac{m_a}{m_p + m_a} \tag{6}$$

$$m_p = \rho_0 \left(1.3R^2 - 5.4Rt_a + 1.7t_a^2\right) t_{exp} \tag{7}$$

$$m_a = \rho_0 \left(2.8Rt_a^2 - 3.9t_a^3\right) \tag{8}$$

In the above shown equations t_a is an effective cell edge thickness value [62], m_a and m_p are, respectively, the polymer weights in the struts and in the cell walls, ρ_0 is the density of the base polymer, Z_f the number of cell walls that face in one edge ($Z_f = 3$), n is the average value of cell walls per cell ($n = 5$) and l is the average length of the cell walls.

On the other side and for a given cell shape in a closed-cell foam, the average cell wall thickness (t) relates to the average cell size (R), to the expansion ratio (ER) and to the mass fraction in the struts (f_s), as shown in the following equation:

$$R(1 - f_s) = Ct\mathrm{ER} \tag{9}$$

where C is a cell-shape dependent constant that takes the value of 3.46 for pentagonal dodecahedron [64] and 3.35 for tetrakaidecahedral cells [65].

Fig. 7 presents the linear regression results of $R(1 - f_s)/\mathrm{ER}$ vs. the average cell wall thickness (t) for the experimental data shown in Table 2. Results fitted well to the previous equation, with a C value of 2.76, suggesting that these foams have comparable cell shapes. Nonetheless, this value indicates that the cells have a different cell shape when compared to pentagonal dodecahedron ($C = 3.46$) and tetrakaidecahedral ($C = 3.35$) shaped cells.

The aspect ratio of the cells (Table 2) resulted slightly higher than 1 for all the samples (AR = 1 for isotropic cells). The hectorite nanoparticles affected the cell shape of the foams, since AR values were lower in the nanocomposite samples. To assess the influence of the hectorite particles on the AR values independently of the expansion ratio, a parameter defined here as the normalized aspect ratio (NAR) was calculated.

$$\mathrm{NAR} = (\mathrm{AR_F} - \mathrm{AR_P})\frac{\mathrm{ER_P}}{\mathrm{ER_F}} \tag{10}$$

where $\mathrm{AR_P}$ and $\mathrm{ER_P}$ are, respectively, the aspect ratio and expansion ratio of the pre-foams, and $\mathrm{AR_F}$ and $\mathrm{ER_F}$ of the foams. The obtained NAR parameter values were 0.21 for PE0, 0.14 for PE3 and 0.09 for PE7, showing that higher hectorite loadings resulted in more isometric cell foams.

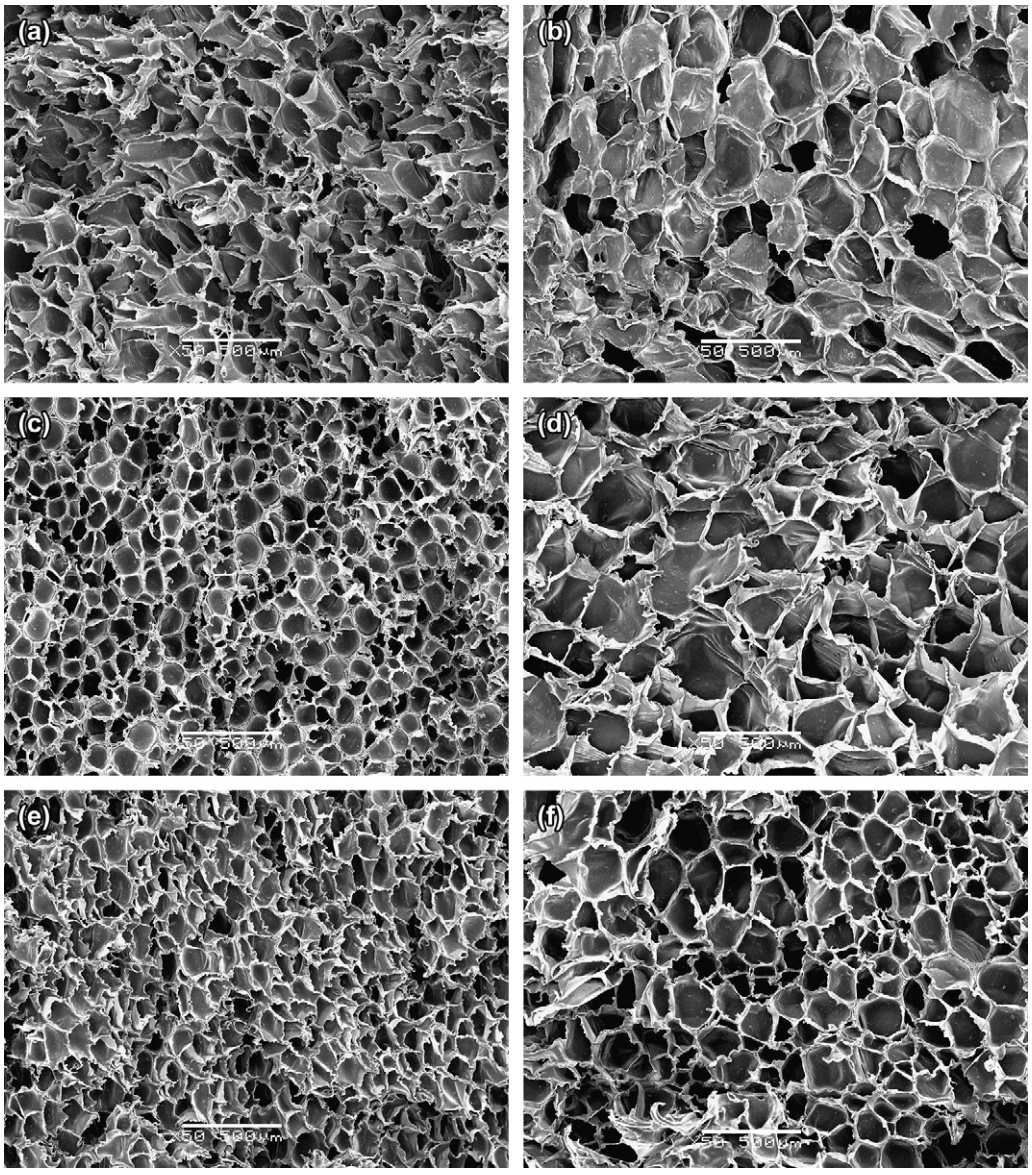

Fig. 5. SEM pictures of (a) PE0-P, (b) PE0-F, (c) PE3-P, (d) PE3-F, (e) PE7-P and (f) PE7-F foamed samples.

3.3. Crystalline characteristics

The X-ray scattering analysis of the samples allowed studying both the exfoliation of the clay particles as well as the polymer crystallinity. WAXS spectra are shown in Figs. 8–10 for all the samples. The hectorite first crystal diffraction peak (peak (001)) appeared for PE3 and PE7 non-foamed samples at lower diffraction angles than that of the organophilized hectorite ($2\theta = 2.4^\circ$ for both hectorite nanocomposites and $2\theta = 3.4^\circ$ for Bentone 108), indicating a partial intercalation of the polyethylene molecules within the clay basal spacing. As a consequence, there was an increase in the interlayer

Table 2
Results of the cellular structure characterization for the pre-foamed and foamed samples

Material	ER	R (μm)	AR	t_{exp} (μm)	t_{theo} (μm)		f_s^{exp}	f_s^{theo}	Cell density (cells/cm^3)
					Model 1	Model 2			
PE0-P	3.2	145	1.56	12.1 ± 1.1	9.3	9.7	0.28	0.24	6.734×10^4
PE3-P	2.8	121	1.12	13.1 ± 1.3	9.9	10.2	0.21	0.20	1.000×10^5
PE7-P	2.6	112	1.42	12.1 ± 3.5	9.6	9.9	0.23	0.23	9.926×10^4
PE0-F	9.3	228	2.17	7.2 ± 1.7	5.7	5.9	0.20	0.16	3.671×10^4
PE3-F	11.9	240	1.72	6.4 ± 0.8	4.5	4.7	0.23	0.17	2.657×10^4
PE7-F	14.2	185	1.58	10.7 ± 1.5	7.8	8.1	0.31	0.30	5.171×10^4

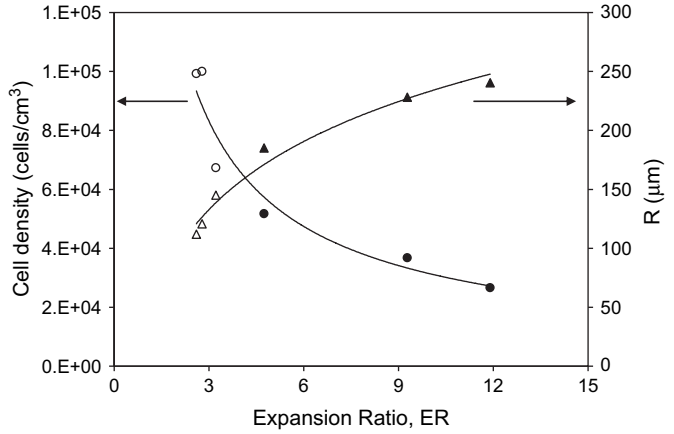

Fig. 6. Cell density and average cell size as a function of the expansion ratio. Hollow symbols correspond to the pre-foams and filled symbols to the foams.

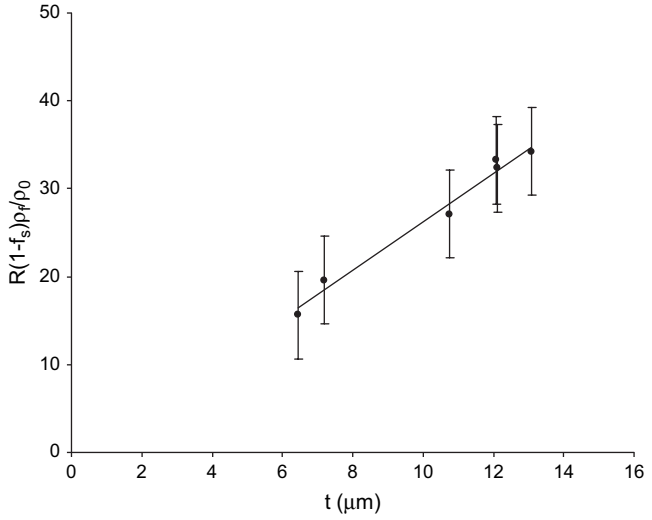

Fig. 7. Experimental results of $R\cdot(1-f_s)\cdot\rho_f/\rho_0$ vs. average cell wall thickness (t) for the LDPE nanocomposite foams.

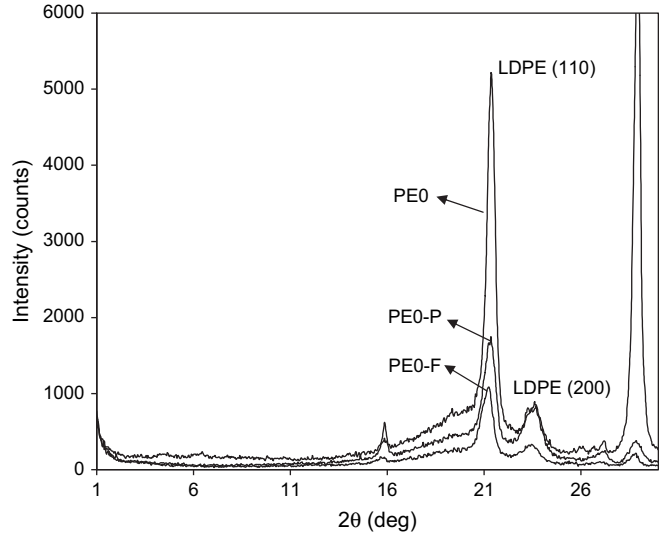

Fig. 8. WAXS spectra of non-foamed, pre-foamed (P) and foamed (F) PE0 samples.

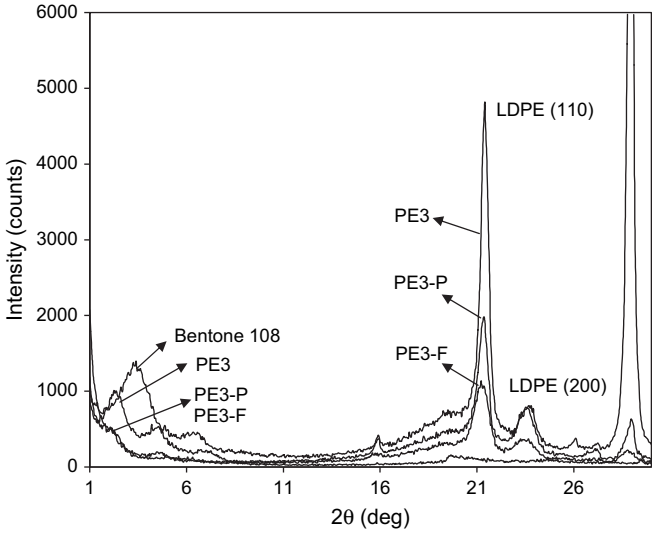

Fig. 9. WAXS spectra of non-foamed, pre-foamed (P) and foamed (F) PE3 samples.

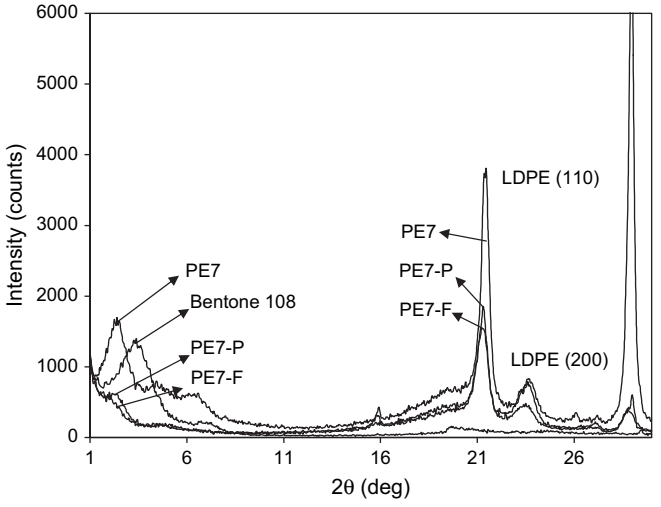

Fig. 10. WAXS spectra of non-foamed, pre-foamed (P) and foamed (F) PE7 samples.

distance from 2.5 nm of the chemically modified pure hectorite to 3.68 nm. As expected, the intensity of the diffraction peak increased with the percentage of hectorite. Nevertheless, the melt-mixing compounding process was not enough to promote an exfoliation of the hectorite particles, only achieved during the pre-foaming process, as seen in Figs. 9 and 10, where the hectorite crystal (001) peak still appeared for the compounded non-foamed nanocomposites. This diffraction signal practically disappeared with the pre-foaming step for both hectorite nanocomposites (PE3-P and PE7-P). The foaming second step did not produce much of a different exfoliated hectorite nanocomposite when compared to the pre-foaming samples.

The diffraction peak at 28° was assigned to ADC, meaning that for PE0, PE3 and PE7 foamed samples a certain degree of the foaming agent remained without decomposing.

Table 3
Typical WAXS and DSC values for the non-foamed, pre-foamed (P) and foamed (F) PE0, PE3 and PE7

Sample	DSC				WAXS	
	Crystallization		Melting		(110) FWHM	X_c (%)
	T_c^p (°C)	X_c^c (%)	T_m^p (°C)	X_c^m (%)		
PE0	96.7	33.1	111.7	30.8	0.471	47.4
PE0-P	96.0	30.8	111.4	29.7	0.674	36.7
PE0-F	95.0	31.0	110.4	28.9	0.696	37.4
PE3	96.6	33.0	111.1	30.1	0.460	49.1
PE3-P	96.0	32.3	110.7	30.8	0.570	38.3
PE3-F	94.9	28.6	110.6	26.9	0.820	37.1
PE7	95.6	34.0	110.4	31.9	0.470	46.0
PE7-P	95.6	31.6	111.1	30.0	0.530	37.2
PE7-F	94.2	29.9	110.5	28.2	0.710	37.1

The LDPE crystallinity degree calculated from the diffraction spectra is shown in Table 3 for all the samples decreased with the foaming process, but not with the presence of hectorite. The lowering of crystallinity was attributed to different polymer crosslinking degrees. Subsequent foaming (second step) did not further decrease the crystallinity percentage, allowing to say that LDPE crystallinity decreased due to higher crosslinking.

To obtain information about the polymer crystallinity perfection, the full width at half maximum (FWHM) was determined for the LDPE (110) peak. Higher values were obtained for the foamed samples, indicating less crystal perfection, associated to the polymer crosslinking degree. The presence of the hectorite nanoparticles did not seem to modify considerably the FWHM values.

DSC results (Table 3) also showed a decrease in crystallinity from the non-foamed to the foamed samples, independently of the hectorite particles. In addition, the crystallization and melting peak temperatures slightly decreased in the samples with the expansion ratio. Again, polymer crosslinking was the cause of these effects.

3.4. Nanocomposite morphology

The TEM analysis showed that the typical morphology of the foamed nanocomposite consisted of mixed dispersed individual hectorite and stacks of hectorite platelets (Fig. 11). First

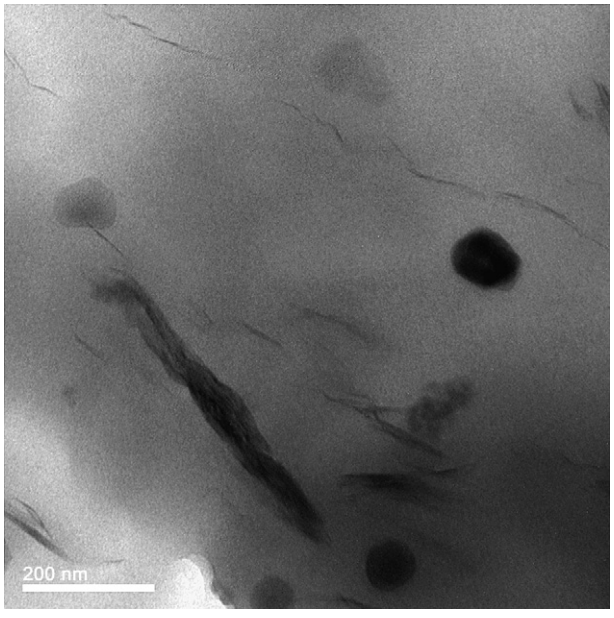

Fig. 11. Typical TEM picture of the foamed 3 wt.% and 7 wt.% nanocomposites.

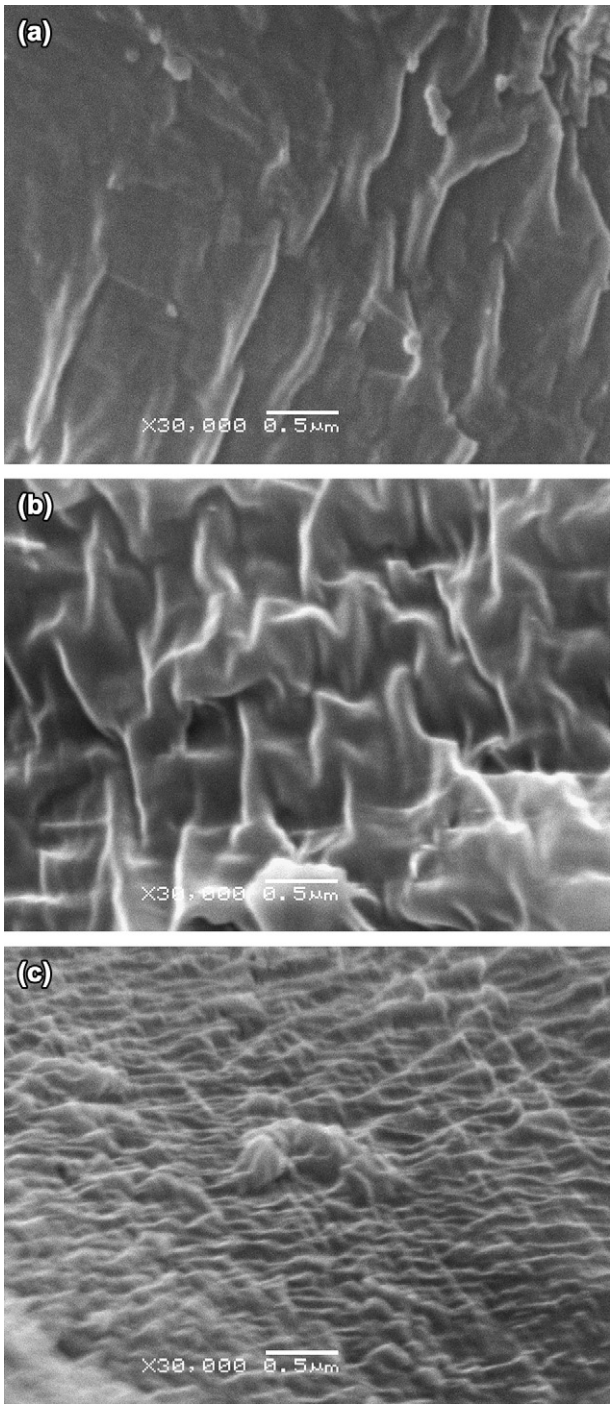

Fig. 12. SEM pictures of the cell wall of (a) PE0, (b) PE3 and (c) PE7 foamed samples.

of all, this morphology was in good agreement with the disappearing of the X-ray hectorite (001) diffraction peak, meaning that the hectorite particles were mainly exfoliated during foaming. Secondly, the presence of these stacks of hectorite platelets could partially explain, together with the differences in crosslinking degree stated previously, the less isotropic expansion of the nanocomposite foams when compared to the neat LDPE ones. As it can be seen from Fig. 11, foaming agent decomposition residues were also present in the form of regular particles of typical size 50 nm.

Observation by SEM of the LDPE foam cell wall showed the typical prints of the polymer texture. As shown in Fig. 12, nanocomposite foams with higher hectorite loadings showed prints with a smaller size and in higher number, presenting a finer texture. This different texture was accounted to local confinement of the polymer caused by the hectorite particles.

4. Conclusions

The effects of the hectorite nanoparticles presence and the foaming behaviour of low density polyethylene closed-cell foams were studied.

Because of the interaction between the polymer molecules and hectorite particles, higher pre-foaming temperatures were needed in the nanocomposites to reach density values similar to those of the PE0 foams.

Higher hectorite loadings resulted in more isometric foams in terms of the cell aspect ratio. The average cell size and the cell density of the foams were found to be independent of the hectorite nanoparticles. The average cell wall thickness decreased for higher expansion ratios, but also seemed unaffected by the presence of hectorite. All the foams presented typical values of mass fraction in the struts, independent of the expansion ratio and hectorite concentration. The foamed nanocomposites underwent faster collapsing when compared to the PE0 foams, related to a lower crosslinking degree of the polymer matrix in the nanocomposites.

LDPE crystallinity was not affected by the hectorite particles, decreasing due to the polymer crosslinking, mainly reached during the pre-foaming step. As a consequence, the crystallization and melting peak temperatures slightly decreased for all the samples with the expansion ratio.

The melt-mixing process used to compound the samples produced intercalated nanocomposites. Considerable exfoliation of the hectorite particles was achieved during the early stages of the foaming process (pre-foaming). The hectorite nanoparticles also seemed to affect the cell wall texture of the foams.

All these remarks and conclusions can be compiled in the fact that not only the foaming process affects the delamination of the hectorite particles, helping to create a nanocomposite type of structure, but also exfoliation changes the morphology of the foams (cell size, distribution and shape), as well as their foaming behaviour. As it is known, shape and distribution of the cells directly affects the bulk properties of the final foamed material (thermal and mechanical properties), and that is why a global cellular characterization as shown in this study is considered to be extremely important.

References

[1] Giannelis EP. Adv Mater 1996;8:29–35.
[2] Giannelis EP, Krishnamoorti R, Manias E. Adv Polym Sci 1999;138:107–47.
[3] LeBaron PC, Wang Z, Pinnavaia TJ. Appl Clay Sci 1999;15:11–29.
[4] Vaia RA, Price G, Ruth PN, Nguyen HT, Lichtenhan J. Appl Clay Sci 1999;15:67–92.
[5] Biswas M, Sinha Ray S. Adv Polym Sci 2001;155:167–221.
[6] Giannelis EP. Appl Organomet Chem 1998;12:675–80.
[7] Bharadwaj RK. Macromolecules 2001;34:1989–92.
[8] Messersmith PB, Giannelis EP. J Polym Sci Part A Polym Chem 1995;33:1047–57.
[9] Ku BC, Froio D, Steeves D, Kim DW, Ahn H, Ratto JA, et al. J Macromol Sci Pure Appl Chem 2004;41(12):1401–10.
[10] Gilman JW, Kashiwagi T, Lichtenhan JD. SAMPE J 1997;33:40–5.
[11] Gilman JW. Appl Clay Sci 1999;15:31–49.
[12] Bourbigot S, LeBras M, Dabrowski F, Gilman JW, Kashiwagi T. Fire Mater 2000;24:201–8.
[13] Gilman JW, Jackson CL, Morgan AB, Harris Jr R, Manias E, Giannelis EP, et al. Chem Mater 2000;12:1866–73.
[14] Vaia RA, Giannelis EP. Macromolecules 1997;30:7990–9.
[15] Lee JY, Baljon ARC, Loring RF, Panagiopoulos AZ. J Chem Phys 1998;109:10321–30.
[16] Balazs AC, Singh C, Zhulina E, Lyatskaya Y. Acc Chem Res 1999;32:651–7.
[17] Ginzburg VV, Balazs AC. Macromolecules 1999;32:5681–8.
[18] Ginsburg VV, Singh C, Balazs AC. Macromolecules 2000;33:1089–99.
[19] Kuznetsov D, Balazs AC. J Chem Phys 2000;112:4365–75.
[20] Lee JY, Baljon ACR, Sogah DY, Loring RF. J Chem Phys 2000;112:9112–9.
[21] Singh C, Balazs AC. Polym Int 2000;49:469–71.
[22] Lee YH, Zheng WG, Park CB, Kontopoulou M. SPE, ANTEC, Technical Papers, Boston; May 1–4 2005, Paper 102105.
[23] Sinha Ray S, Okamoto M. Prog Polym Sci 2003;28:1539–641.
[24] Hackett E, Manias E, Giannelis EP. J Chem Phys 1998;108:7410–5.
[25] Anastasiadis SH, Karatasos K, Vlachos G, Manias E, Giannelis EP. Phys Rev Lett 2000;84:915–8.
[26] Manias E, Kuppa V. Colloids Surf A 2001;187–188:509–21.
[27] Gopakumar TG, Lee JA, Kontopoulou M, Parent JS. Polymer 2002;43:5483–91.
[28] Koo CM, Ham HT, Kim SO, Wang KH, Chung IJ, Kim DC, et al. Macromolecules 2002;35:5116–22.
[29] Morawiec J, Pawlak A, Slouf M, Galeski A, Piorkowska E, Krasnikowa N. Eur Polym J 2005;41:1115–22.
[30] Almanza OA, Rodríguez-Pérez MA, de Saja JA. Polymer 2001;42:7117.
[31] Rodríguez-Pérez MA. Adv Polym Sci 2005;184. 1-x (Published online).
[32] Puri RR, Collington KT. Cell Polym 1988;7:219–31.
[33] Sims GLA, Mahapatro A. Structure/process/property relationships in molded polyethylene foams, Annual Technical Conference – ANTEC; 1998.
[34] Velasco JI, Martínez AB. J Mater Sci 1999;34:431–8.
[35] Rodríguez-Pérez MA, Velasco JI, Arencón D, Almanza O, de Saja JA. J Appl Polym Sci 2000;75:156–66.
[36] Velasco JI, Martinez AB, Arencón D, Almanza O, Rodriguez-Perez MA, de Saja JA. Cell Polym 2000;19(2):115–33.
[37] Zeng C, Han X, James Lee L, Koelling KW, Tomasko DL. Adv Mater 2003;15(20).
[38] Colton JS, Suh NP. Polym Eng Sci 1987;27:493.
[39] Goel SK, Beckman EJ. Polym Eng Sci 1994;34:1137.
[40] Lee YH, Park CB, Wang KH, Lee MH. SPE, ANTEC, Technical Papers, Boston; May 1–4 2005, Paper 102100.
[41] Zheng WG, Lee YH, Park CB. The effects of nanoclay on extrusion microcellular foaming of nylon. SAE International; 2004.

[42] Winter HH, Gappert G, Ito H. Macromolecules 2002;35:3325.
[43] Ramesh NS, Rasmussen DH, Campbell GA. Polym Eng Sci 1994;34:1685.
[44] Sims GLA, Sirithongtaworn W. Cellular Polymers III, RAPRA Coventry; April 1995, Paper 23.
[45] Sims GLA, Khunniteekool C. Cell Polym 1996;15:1–13.
[46] Sims GLA, Khunniteekool C. Cell Polym 1996;15:14–29.
[47] Mahapatro A, Mills NJ, Sims GLA. Cell Polym 1998;17:252–70.
[48] Abe S, Yamaguchi M. J Appl Polym Sci 2001;79:2146.
[49] Zhang Y, Rodrigue D, Ait-Kadi A. J Appl Polym Sci 2003;90:2111.
[50] Tai HJ, Wang JB. J Cell Plast 1997;3:304.
[51] Zheng WG, Lee YH, Park CB. SPE, ANTEC, Technical Papers, Charlotte; May 7–11 2006, Paper 103069.
[52] Zheng WG, Lee YH, Park CB. SAE World Congress, Detroit, April 3–6 2006.
[53] Zheng WG, Park CB. SPE, ANTEC, Technical Papers, Boston; May 1–4 2005, Paper 100839.
[54] Zhang J, Jiang DD, Wilkie CA. Thermochim Acta 2005;430:107.
[55] ASTM D1622, Annual Book of ASTM Standards, vol. 8.01. 1998.
[56] ASTM D2675–90, Annual Book of ASTM Standards, vol. 8.01. 2001.
[57] Sims GLA, Khunniteekool C. Cell Polym 1994;13:137.
[58] Rodríguez-Pérez MA, Alonso O, Duijsens A, de Saja JA. J Polym Sci Part B Polym Phys 1998;36:2587.
[59] Kuhn J, Ebert HP. Int J Heat Mass Transfer 1992;35:1795.
[60] Mills NJ, Zhu HX. The compression of closed-cell polymer foams. In: Sadoc F, Rivier N, editors. Foams and emulsions. NATO ASI Series. Dordrecht: Kluwer. p. 175.
[61] ASTM D3576, Annual Book of ASTM Standards, vol. 8.02. 1998.
[62] Gibson LJ, Ashby MF. Cellular solids: structure and properties. Oxford: Pergamon Press; 1988. p. 130–332.
[63] Wunderlich B. Thermal analysis. New York: Academic Press; 1990.
[64] Glicksman LR. Low density cellular plastics: physical basis of behaviour. In: Hilyard NC, Cunningham A, editors. London: Chapman and Hall; 1994.
[65] Mills NJ, Gilchrist AJ. Cell Plast 1997;33:264.